Int. J. Heat Mass Transfer. Vol. 34, No. 7, pp. 1755–1771, 1991
Printed in Great Britain

0017-9310/91 $3.00+0.00

A study of steady-state steam–water counterflow in porous media

C. SATIK, M. PARLAR and Y. C. YORTSOS†

Departments of Petroleum and Chemical Engineering, University of Southern California, Los Angeles, CA 90089-1211, U.S.A.

(*Received* 25 *October* 1989 *and in final form* 12 *September* 1990)

Abstract—Vapor–liquid counterflow in porous media arises in processes such as heat pipes, oil recovery and geothermal systems. While previous studies analyzed these processes separately, this paper presents a unified description. The analysis includes capillarity, heat conduction, and Kelvin effects. The importance of each term to the various applications is examined. Significantly, it is found that the critical heat flux in a heat pipe is not constant, but increases with decreasing permeability. A threshold permeability is also identified, below which steady states may not exist. Related conclusions are reached regarding liquid-dominated geothermal systems.

INTRODUCTION

THE STEADY-state counterflow of a liquid and its vapor in porous media arises in many processes driven by temperature gradients. Large scale applications involve geothermal systems [1–4], thermal oil recovery [5], and nuclear waste disposal [6, 7]. Laboratory investigations have concentrated on porous heat pipes [8, 9], boiling [10–12] and drying [13]. All these processes share many common aspects, principally phase equilibria and their interplay with fluid flow, heat transfer and capillarity.

Although a precise description of flow with vapor–liquid equilibria in porous media is not presently available, the conventional approach that vapor and liquid phases obey Darcy's law with saturation-dependent permeabilities is often considered adequate. Steady-state vapor–liquid flows in porous media have been modeled with such methodology for several decades [14]. Recent applications to steam–water counterflow include studies by Martin *et al.* [15], Schubert and Straus [16], Bau and Torrance [17] and Udell [18, 19]. The first two papers focused on geothermal applications, thus they neglected capillarity, but included heat conduction. By contrast, Udell [18, 19] considered heat pipes, in which capillarity predominates, but conduction is neglected. In the same context, Bau and Torrance [17] presented a simplified analysis, where both conduction and capillarity are negligible.

While these studies have been instrumental in the understanding of vapor–liquid counter-flow, several issues are still obscure. In the context of heat pipes, the interplay between capillarity and heat conduction is unresolved, particularly in regards to the critical heat flux. The latter is appropriate to bottom heating and it is defined [17, 19] as the minimum heat flux value for the occurrence of dry-out, that is for a vapor zone to exist at the heated end. The characterization of flow regimes is incomplete for heat fluxes lower than the critical, where present models predict an infinite, two-phase zone of constant saturation. Finally, the importance of Kelvin effects is unclear. While vapor pressure lowering due to capillarity is frequently used in such models [18, 20, 21], its practical relevance has not been assessed. In the context of geothermal systems, the possible existence of two flow regimes (vapor- and liquid-dominated) has long been proposed [15]. It is not clear, however, whether both regimes are indeed acceptable, and what are the selection criteria.

Part of the difficulty lies in previous approximations, which break down in various regions. To alleviate this problem, a more detailed study is necessary. This forms the main objective of this paper. Also recognizing the fact that previous studies in heat pipes and in geothermal problems are different applications of essentially the same process (although temperature gradients, thus flow directions, may be of opposite sign) a common formalism should be possible. For this reason, we consider a complete formulation that includes capillarity, heat conduction, phase equilibria that includes vapor pressure lowering.

The flow model is taken to be an extension of Darcy's law with the use of relative permeabilities, and allows for vapor pressure lowering due to Kelvin effects. Both representations are based on the premise of capillary control at the pore level, usually enforced for low values of capillary and Bond numbers, and when temperature gradients are relatively low. The assumption that pore wall curvature stabilizes vapor–liquid interfaces is implicit. Such conditions are necessary for a description in terms of saturation-dependent relative permeabilities and capillary pressure functions. Precise criteria for their validity are

† Author to whom correspondence should be addressed.

NOMENCLATURE

A	dimensionless vapor pressure
b	dimensionless Kelvin group
g	gravitational constant [L T^{-2}]
J	dimensionless capillary pressure
k	permeability [L^2]
K	$(L_v/M_w)/T_0R$) [dimensionless]
L_v	latent heat [L^{2}T^{-2}]
$\dot{m}$	dimensionless evaporation rate
M_w	molecular weight of water [Mmol^{-1}]
n	permeability exponent [dimensionless]
P	pressure [M L^{-1}T^{-2}]
q_h	heat flux [M T^{-3}]
R	gas constant [L^{2}T^{-2}mol^{-1}K]
R_c	$(k\rho_V L_v\sigma)/(\mu_V\sqrt{k}\lambda_{II}T_0)$ [dimensionless]
R_h	$(q_h\sigma)/(\lambda T_0\sqrt{kg\Delta\rho})$ [dimensionless]
R_l	$\rho_L/\Delta\rho$ [dimensionless]
R_μ	μ_L/μ_V [dimensionless]
R_m	$(kL_vP_{V0}(T_0)\rho_V)/(\mu_V\lambda_{II}T_0)$ [dimensionless]
R_p	$(P_{V0}(T_0)\sqrt{k})/(\sigma)$ [dimensionless]
R_ρ	ρ_V/ρ_L [dimensionless]
R_v	$\rho_V/\Delta\rho$ [dimensionless]
S	saturation [dimensionless]
T	temperature [K]
v_L	liquid molar volume [L^{3}mol^{-1}]
V	volumetric flow rate (L T^{-1}].

Greek symbols

β	R_μ/R_ρ
Γ	temperature gradient [K L^{-1}]
ε	$1/KR_p$ [dimensionless]
θ	angle of inclination [deg]
λ	thermal conductivity [M L T^{-3}K^{-1}]
μ	viscosity [M L^{-1}T^{-1}]
ξ	dimensionless distance
ρ	density [M L^{-3}]
$\Delta\rho$	$\rho_L-\rho_V$ [M L^{-3}]
σ	surface tension [M T^{-2}]
τ	temperature [dimensionless]
ω	heat flux [dimensionless].

Subscripts

b	threshold
c	capillary
cr	critical
L	liquid
r	relative
V	vapor
V0	saturation
0	reference
I	region I
II	region II
III	region III.

Superscript

o	outer solution.

currently under development, that parallel related problems of bubble growth in porous media [22].

We first derive a general dimensionless representation, for steady-state, vapor–liquid counterflow. The heat pipe and geothermal problems are subsequently obtained as special cases and they are analyzed in separate sections. We identify the former as the limit of small conduction and the latter as the limit of small capillarity. Hence, we investigate boundary layers due to vapor pressure lowering and heat conduction in the first case, and due to capillarity in the latter. The nature of the critical heat flux for bottom heating in a heat pipe problem, and its dependence on process parameters are examined in detail. Finally, for both heat pipe and geothermal problems we identify regimes, where steady-state counterflow may not exist.

FORMULATION

We consider the steady state, one-dimensional, countercurrent flow of a single component, two-phase, liquid–vapor (e.g. steam–water) system. As a result of an externally imposed heat flux q_h, three regions develop [18]: two no-flow regions (I and III in Fig. 1) containing mostly vapor or liquid, respectively, and an intermediate two-phase region (II), where counterflow occurs. In our notation, the space coordinate x increases in the direction from the liquid to the vapor. The system is inclined at an angle θ with respect to the horizontal, such that vapor is at the top when $0 < \theta < \pi$, and at the bottom otherwise, $\pi < \theta < 2\pi$.

Momentum balances for the fluid phases are described by Darcy's law

$$V_{Lx} = -\frac{k}{\mu_L}k_{rL}\left(\frac{\partial P_L}{\partial x} + \rho_L g\sin\theta\right) \quad (1)$$

$$V_{Vx} = -\frac{k}{\mu_V}k_{rV}\left(\frac{\partial P_V}{\partial x} + \rho_V g\sin\theta\right) \quad (2)$$

where the relative permeabilities k_{rL} and k_{rV} depend on the liquid saturation, S. This formulation ignores viscous coupling, that may be present in countercurrent flows [23]. The two pressures are related via the capillary pressure function

$$P_V - P_L = P_c(S) = \frac{\sigma}{\sqrt{k}}J(S) \quad (3)$$

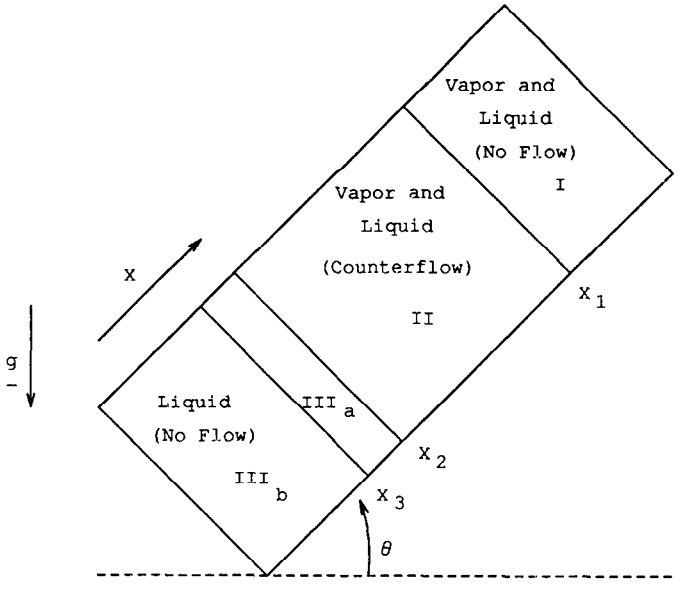

FIG. 1. Countercurrent flow schematic.

where a typical representation in terms of a Leverett J function was introduced.

Salient features of relative permeabilities for vapor–liquid systems are discussed elsewhere, following a percolation approach [20, 22], where the roles of pore space geometry and topology are emphasized. The residual saturation values (S_{Lr}, S_{Vr}), below which bulk flow of the respective phases ceases (k_{rL}, k_{rV} vanish, respectively), should be noted. In the ensuing discussion use will be made of the simple, although *ad hoc*, numerical expressions of Table 1.

Table 1. Typical parameter values

$S_{Lr} = 0.20$
$S_{Vr} = 0.05$
$T_0 = 171.1\ ^\circ C$
$P_0 = 15$ psi
$\sigma = 58.91$ dyn cm^{-1}
$v_L = 18.76$ cm^3 mol^{-1}
$\rho_L = 0.9606$ g cm^{-3}
$\rho_V = 0.0006$ g cm^{-3}
$\mu_L = 2.824 \times 10^{-3}$ g cm^{-1} s^{-1}
$\mu_V = 1.260 \times 10^{-4}$ g cm^{-1} s^{-1}
$\lambda_I = 3.0$ W m^{-1} K^{-1}
$\lambda_{III} = 1.2$ W m^{-1} K^{-1}
$\lambda_{II} = \frac{\lambda_I - \lambda_{III}}{2}(1 - S_{Vr} - S_{Lr}) + \lambda_{III}$
$k_{rL} = \left(\frac{S - S_{Lr}}{1 - S_{Lr}}\right)^3$
$k_{rV} = \left(\frac{1 - S_{Vr} - S}{1 - S_{Vr}}\right)^3$
$P_c = 2.24 - 2.75S + 1.3S^2$

We subsequently take

$$P_V = P_{V0}(T) \exp\left(-\frac{v_L}{RT} P_c(S)\right) \tag{4}$$

to describe pressure lowering, and use the Clausius–Clapeyron formula

$$P_{V0}(T) = P_{V0}(T_0) \exp\left(\frac{L_v M}{R}\left(\frac{1}{T_0} - \frac{1}{T}\right)\right) \tag{5}$$

for phase equilibria. Mass and thermal energy balances complete the formulation

$$\rho_L V_{Lx} + \rho_V V_{Vx} = 0 \tag{6}$$

$$\rho_V L_V V_{Vx} + q_h = \lambda \frac{\partial T}{\partial x} \tag{7}$$

where all fluid properties are taken independent of P and T. Due to different flow behavior the three different regions (Fig. 1) are examined separately.

No-flow regions (I and III)

Region I is a no-flow, mostly vapor-occupied zone, where

$$0 \leqslant S \leqslant S_{Lr} \tag{8}$$

thus $k_{rL}(S) = 0$, $V_{Lx} = 0$ and, from equation (6), $V_{Vx} = 0$. At the residual value S_{Lr}, bulk liquid in the pore space becomes disconnected, and bulk flow ceases. The liquid being strongly wetting, keeps hydraulic continuity in the form of thin film flow, however, even for $S < S_{Lr}$. These rates are quite low and will not be considered here. Thus, the pressure of the vapor phase is hydrostatic and the temperature distribution linear

$$P_V = P_1 - \rho_V g x \sin\theta \tag{9}$$

$$T = T_1 + q_h x/\lambda_1 \tag{10}$$

where P_1, T_1 are constants. A saturation profile results

$$J(S) = \frac{1}{b}\ln\left(\frac{P_{V0}(T_1 + q_h x/\lambda_1)}{P_1 - \rho_V g x \sin\theta}\right) \tag{11}$$

where the dimensionless group $b = \sigma v_1 / RT\sqrt{k}$ parametrizes Kelvin effects. For media of practical interest ($b \ll 1$), the liquid is at low saturation ($J(S) \gg 1$) in most of region I, and exists in a pendular state where effects of thin films are predominant. Recent works [24, 25] have elucidated the capillary pressure–saturation relationship in this regime for non-condensing flows. In this paper, such effects are not considered. The extent (x_1) of the vapor zone I is demarcated by setting $S = S_{1r}$ in equation (11). For $b \ll 1$, one may further approximate

$$P_{V0}(T_1 + q_h x_1/\lambda_1) \simeq P_1 - \rho_V g x_1 \sin\theta \tag{12}$$

which is the condition for vapor saturation, and determines the boundary of the two regions I, II. The sharp saturation rise to the residual value S_{1r} near the boundary (where the logarithm in equation (11) becomes of order b) should be noted.

Likewise, region III is a no-flow, mostly liquid-occupied zone, where

$$1 - S_{Vr} \leqslant S \leqslant 1 \tag{13}$$

thus, $k_{rV}(S) = 0$, $V_{Vx} = 0$, and, from equation (7), $V_{1x} = 0$. Pressure and temperature profiles are linear

$$P_1 = P_{III} - \rho_L g x \sin\theta \tag{14}$$

$$T = T_{III} + q_h x/\lambda_{III} \tag{15}$$

with P_{III}, T_{III} appropriate constants. However, in contrast to region I, where a saturation profile exists due to the liquid wetting, the bulk of region III (IIIb in Fig. 1) is at $S = 1$. Saturation changes are confined within a narrow domain (IIIa), the boundary of which (x_3) is the solution of $P_c = 0$

$$P_{V0}(T_{III} + q_h x_3/\lambda_{III}) = P_{III} - \rho_L g x_3 \sin\theta. \tag{16}$$

To the left lies boundary x_2, obtained by taking $S = 1 - S_{Vr}$

$$P_{V0}(T_{III} + q_h x_2/\lambda_{III}) = P_{III} - \rho_L g x_2 \sin\theta + \frac{\sigma}{\sqrt{k}} J(1 - S_{Vr}) \tag{17}$$

and where Kelvin effects were neglected without loss.

Flow region

The region of two-phase, countercurrent flow is the most interesting. Saturation and temperature profiles are described by two coupled equations by combining equations (1)–(7). After considerable algebra, the following is obtained:

$$\frac{d\tau}{d\xi} = \frac{H(\tau, S)}{F(\tau, S)} \tag{18}$$

$$\frac{dS}{d\xi} = \frac{G(\tau, S)}{F(\tau, S)\dfrac{dJ}{dS}} \tag{19}$$

where dimensionless notation has been used, with ξ denoting distance normalized by $\sigma/\sqrt{(k)}g\Delta\rho$, and τ denoting temperature normalized by a reference temperature T_0. The functions H, F, and G are given respectively by

$$H = k_{rL}[(1 + bR_p A)R_h + \sin\theta k_{rV}(bR_m A - R_v R_c)] + bk_{rV}\beta R_p R_h A \tag{20}$$

$$F = k_{rL}\left[1 + bR_p A + k_{rV} K R_m \frac{A}{\tau^2}\right] + bk_{rV}\beta R_p A \tag{21}$$

and

$$G = k_{rL}\left[\sin\theta R_1 + KR_p R_h \frac{A}{\tau^2} + \sin\theta k_{rV} K R_m \frac{A}{\tau^2}\right] + \beta k_{rV}\left[\sin\theta R_v + KR_p R_h \frac{A}{\tau^2}\right]. \tag{22}$$

Variable A is a vapor pressure normalized by the saturation pressure at T_0 and includes Kelvin effects

$$A = \exp\left(K\left(1 - \frac{1}{\tau}\right) - bJ(S)\right). \tag{23}$$

All dimensionless groups are defined in the Nomenclature and they are functions of the fluid and rock properties, with the exception of

$$R_h = \frac{q_h \sigma}{\lambda_{II} T_0 \sqrt{(k)} g\Delta\rho} \tag{24}$$

which is a measure of the imposed heat flux, and is simply related to the parameters ω or Γ defined in ref. [18] or ref. [16], respectively

$$\omega = \frac{R_p R_h}{R_m} = \frac{\lambda_{II}\Gamma\mu_V}{kL_V g\Delta\rho\rho_V}. \tag{25}$$

The above constitutes an initial value problem to be solved subject to appropriate initial conditions. The latter vary according to the application. For the heat pipe problem [18] we take

$$\tau = \frac{T_1}{T_0}; \quad S = S_{1r} \quad \text{at} \quad \xi = \xi_1 \tag{26}$$

where $T_1 = T_0 + q_h x_1/\lambda_1$, the reference temperature T_0 corresponds to the (dry) end of the vapor zone, and the integration is in the direction of decreasing ξ. For the geothermal problem [16] the initial condition is

$$\tau = 1; \quad S = 1 \quad \text{at} \quad \xi = 0. \tag{27}$$

The reference temperature T_0 corresponds to the boundary of regions IIIa IIIb, and the integration is in the direction of increasing ξ. Forward integration of equations (18) and (19) subject to equation (26) or (27) uniquely determines saturation and temperature profiles in the two applications.

For future reference the expression for the dimensionless vapor flow velocity V_{Vx}, normalized by $k\Delta\rho g/\mu_V$, is also derived

$$V_{Vx} = -\frac{k_{rV}k_{rL}\left[\sin\theta R_v - bR_pA + KR_pR_h\frac{A}{\tau^2}\right]}{F(\tau,S)}. \tag{28}$$

It must be remarked that, for all practical purposes ($b \ll 1$), the magnitude, but not the sign, of the angle θ can be scaled out in equations (18), (19), and (28), by a simple rescaling of the space variable ξ by $|\sin\theta|$ and of the heat flux term R_h (or ω) by $1/|\sin\theta|$. Thus, it only suffices to study the generic cases $\theta = \pi/2, 3\pi/2$.

Contrasted to the above, and excluding field-scale numerical simulators, present models are quite simple. We refer to Udell [18, 19], for the heat pipe problem and to Schubert and Straus [16], for the geothermal problem. As shown below, these models arise as limiting cases of the present formulation. To facilitate the presentation, however, the two cases will be examined separately. We proceed by applying equations (12)–(28) to the two problems.

HEAT PIPE PROBLEM

In the context of the heat pipe problem we investigate Kelvin and heat conduction effects, and will explore the critical heat flux curve. For this purpose, we will frequently refer to the model in refs. [18, 19], which represents a particular limit of the present model. We shall denote by Θ, Σ, and Ψ the temperature, saturation, and vapor flux, respectively, corresponding to refs. [18, 19]. In our notation, that analysis is tantamount to taking in equations (18)–(28) the limits $b \ll 1$, and $KR_m \gg 1$ with R_h/R_m fixed, the latter condition corresponding to negligible heat conduction. Indeed, at these limits, the vapor flow rate, equation (28), reduces to

$$-V_{Vx} \to \Psi = \omega \tag{29}$$

and the saturation equation (19) becomes uncoupled from temperature

$$J'\frac{d\Sigma}{d\xi} = \sin\theta + \omega\left(\frac{1}{k_{rV}} + \frac{\beta}{k_{rL}}\right). \tag{30}$$

The above two limits place constraints on the validity of previous results. Clearly, the condition for negligible Kelvin effects, $b \ll 1$, is generally well satisfied for most porous media of practical interest (e.g. permeabilities exceeding $O(10^{-15}\ m^2)$). Neglecting heat conduction, on the other hand, requires $KR_m \gg 1$ at fixed R_h/R_m, a significantly tighter restriction (e.g. $k \gg O(10^{-13}\ m^2)$ for the experiment in ref. [18]). As shown in subsequent sections, substantial changes may result when this condition is not satisfied. We proceed, first, by examining the effects of the two constraints on saturation and temperature profiles.

Boundary layer analysis

As a consequence of conditions $b \ll 1$, $KR_m \gg 1$ two boundary layers arise at the ends of region II. This is evident from expression (29) which dictates a step change in the vapor flux, thus infinitely large evaporation–condensation rates, at the boundaries. In actuality, the vapor flux vanishes smoothly at the two boundaries (where the two relative permeabilities also vanish). This feature is retained in the present formulation, as can be seen from an expansion of the full expression (28)

$$V_{Vx} \sim \begin{cases} -\dfrac{k_{rL}KR_h}{b\beta\tau^2}; & S \to S_{Lr} \\ -\dfrac{k_{rV}KR_pR_hA}{\tau^2}; & S \to 1 - S_{Vr} \end{cases}. \tag{31}$$

The singular behavior of expression (31) in the respective limits ($b \ll 1, KR_m \gg 1$) is apparent. We shall analyze the solution in the two boundary regions. Near the dry zone the more general case $b \ll 1$, finite KR_m, is considered.

(i) *Case $b \ll 1$, finite KR_m*

Here, a boundary layer in the vapor flux develops at the evaporating end (near S_{Lr}). The outer solution outside this layer (superscript (o)) is obtained by neglecting Kelvin effects in equations (18), (19), and (28)

$$\frac{d\tau^{(o)}}{d\xi} = \frac{R_h - k_{rV}R_vR_c\sin\theta}{1 + k_{rV}\dfrac{KR_mA}{(\tau^{(o)})^2}} \tag{32}$$

$$\frac{dS^{(o)}}{d\xi} = \frac{G(\tau^{(o)}, S^{(o)})}{k_{rL}\left(1 + k_{rV}\dfrac{KR_mA}{(\tau^{(o)})^2}\right)J'(S^{(o)})} \tag{33}$$

$$V_{Vx}^{(o)} = -\frac{\sin\theta\, k_{rV}\left[R_v + KR_pR_h\dfrac{A}{(\tau^{(o)})^2}\right]}{1 + k_{rV}\dfrac{KR_mA}{(\tau^{(o)})^2}}. \tag{34}$$

Near S_{Lr}, the saturation (although not the temperature) gradient diverges, thus a change of scales is needed. By taking the typical expansion, $k_{rL} \sim L(S - S_{Lr})^n$, where $L > 0$ is constant and $n > 1$, we rescale

$$S = S_{Lr} + b^{\alpha}\sigma(z) \tag{35}$$

$$\xi = \xi_t - b^{\kappa}z \tag{36}$$

with $\alpha, \kappa > 0$ to be determined. Substitution into the full equations (18) and (19), subsequent expansion and use of the dominant balance [26] results in

$$\alpha = \frac{1}{n} \tag{37}$$

$$\kappa = 1 + \frac{1}{n}. \tag{38}$$

In this asymptotic technique the set of exponents is

uniquely determined such that the singular behavior of the outer solution is eliminated. It follows that the (evaporation) boundary layer is of the order $b^{1+1/n}$. Furthermore, the saturation profile within the layer can be constructed by substitution and integration

$$\sigma+\frac{\sigma^{n+1}}{(n+1)c}=-ez. \tag{39}$$

The corresponding vapor flux in the boundary layer is obtained from equation (28) by substitution of equations (35) and (36)

$$V_{\mathrm{V}x}=\frac{V_{\mathrm{V}x}^{(\mathrm{o})}(S_{\mathrm{Lr}})}{1+c\sigma^{n}}. \tag{40}$$

This expression correctly predicts that inside the boundary layer, $V_{\mathrm{V}x}$ varies smoothly, by vanishing at the one end ($\sigma=0$) and by asymptotically approaching the outer value, $V_{\mathrm{V}x}^{(\mathrm{o})}(S_{\mathrm{Lr}})$, at the other ($\sigma\to\infty$) (Fig. 2). Likewise, the dimensionless evaporation rate $\dot{m}=\mathrm{d}V_{\mathrm{V}x}/\mathrm{d}\xi$ can be evaluated

$$\dot{m}=\frac{f\sigma^{n-1}}{b^{1+1/n}\left[1+\dfrac{\sigma^{n}}{c}\right]^{3}} \tag{41}$$

where c, e, and f are process constants (Appendix). A normalized plot is shown in Fig. 2. It is noted that in this approximation ($b\ll 1$) all evaporation takes place within the boundary layer, $\dot{m}$ increasing to a maximum value, before rapidly decaying to zero at the other end of the boundary layer ($z\to+\infty$). As shown in equation (41), the local rates intensify for smaller values of b, for example when the permeability increases, such that, however, the total evaporation rate remains finite

$$I=\int_{0}^{+\infty}b^{1+1/n}\dot{m}\,\mathrm{d}z=-\frac{fc}{en}. \tag{42}$$

Of course, the latter equals the jump in the outer value $V_{\mathrm{V}x}^{(\mathrm{o})}(S_{\mathrm{Lr}})$, which is discontinuous at S_{Lr}.

The above analysis shows that in most practical cases ($b\ll 1$) the evaporation region is a thin layer of order $b^{1+1/n}$ at the interface between dry and two-phase zones. Outside this layer in region II, Kelvin effects are insignificant, and the process is well described by the outer solutions (18), (32), and (34). In particular, an analysis of the latter equation shows that the vapor flux magnitude $|V_{\mathrm{V}x}^{(\mathrm{o})}|$ continuously decreases, as S increases, suggesting that condensation occurs over the entire two-phase zone, and not strictly at the end, as normally assumed. Of course, local condensation rates depend on the value of KR_{m}. For large values of the latter, as implicitly taken in refs. [18, 19], condensation is restricted on a boundary layer at the interface between liquid and two-phase zones. This boundary layer is due to heat conduction alone.

(ii) *Case* $b\ll 1$, $KR_{\mathrm{m}}\gg 1$, $R_{\mathrm{h}}/R_{\mathrm{m}}$ *finite*

In this no-conduction limit, the outer solutions (Θ, Σ, and Ψ) are given by expressions (29) and (30) and by

$$R_{\mathrm{p}}\frac{\mathrm{d}\Theta}{\mathrm{d}\xi}=\frac{\omega-k_{\mathrm{rV}}R_{\mathrm{v}}\sin\theta}{\dfrac{KA}{\Theta^{2}}k_{\mathrm{rV}}}. \tag{43}$$

Under the tacit assumption $b\ll\delta\equiv 1/KR_{\mathrm{m}}$, the previous analysis holds, and only the boundary layer near $1-S_{\mathrm{Vr}}$ needs to be considered. Now, however, the temperature gradient also diverges. To proceed, we

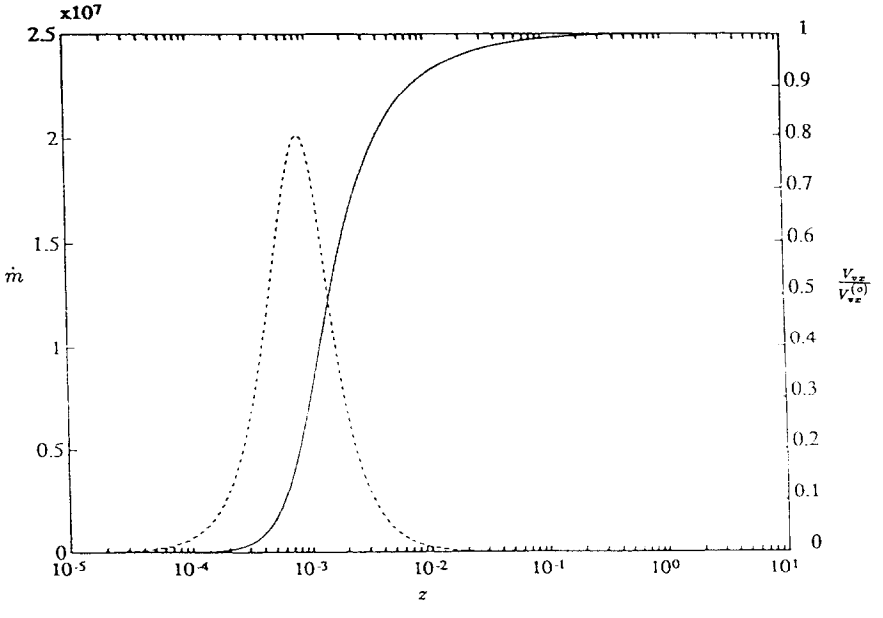

FIG. 2. Boundary layer profiles: normalized vapor flux and evaporation rate.

first note that, to first-order, the boundary temperature at ξ_2 is given by the outer solution by combination of equations (33) and (43) and integration

$$R_p(A_2-A_1)=\omega\int_{S_{Lr}}^{1-S_{Vr}}\frac{\left(1-\dfrac{k_{rv}R_v\sin\theta}{\omega}\right)J'(S)\,dS}{k_{rV}\left[\sin\theta+\omega\left(\dfrac{1}{k_{rV}}+\dfrac{\beta}{k_{rL}}\right)\right]}. \tag{44}$$

Here $A=\exp[K(1-1/\Theta)]$ and it was implied that the denominator does not vanish (but see also below). Next, we rescale saturation, spatial distance and temperature as before

$$S=1-S_{Vr}-\delta^{\alpha}\sigma(z) \tag{45}$$

$$\xi-\xi_2=\delta^{\kappa}z \tag{46}$$

$$\Theta=\Theta_2+\delta^{\gamma}\eta(z) \tag{47}$$

to obtain with the use of dominant balance

$$\alpha=\gamma=\frac{1}{m} \tag{48}$$

$$\kappa=1+\frac{1}{m} \tag{49}$$

where m is the exponent in the permeability expansion $k_{rV}\sim M(1-S-S_{Vr})^m$. The rescaled saturation satisfies the equation

$$\frac{d\sigma}{dz}=-\frac{\omega G}{J'(1-S_{Vr})[1+MG\sigma^m]} \tag{50}$$

where $G=A_2/\Theta_2^2$. An analysis similar to the previous one also applies, and identical results can be reached regarding condensation rates. For example, the vapor flux inside the boundary layer has the form

$$V_{Vx}=-\frac{\omega}{1+\dfrac{\sigma^{-m}}{LG}} \tag{51}$$

which correctly predicts that V_{Vx} vanishes at $1-S_{Vr}$ ($\sigma=0$), while it approaches the asymptotic value $-\omega$ in the outer limit ($\sigma\to\infty$). We omit further details and only mention that at such conditions, vapor condensation is restricted in a boundary layer of width $\delta^{1+1/m}$ at the end of the two-phase zone. The boundary location and the boundary temperature are accurately approximated at large KR_m from the outer solutions. The temperature drop across the two-phase region is given by equation (44), which reflects solely the interaction between capillarity and phase change.

We conclude that in general cases of practical interest ($b\ll 1$) evaporation occurs only within a boundary layer in the vicinity of the vapor zone, outside of which vapor pressure lowering due to Kelvin effects can be neglected. By contrast, condensation is driven by heat conduction and, unless $\delta=1/KR_m\ll 1$, it may not be neglected in the bulk of the two-phase zone. In several practical applications, KR_m is not necessarily large, thus previous results [17–19] may be inapplicable. The effect is most significant in the estimation of the critical heat flux as discussed in the next section.

Critical heat flux

Critical heat flux was defined as the minimum flux above which dry-out occurs and a two-phase zone exists [17, 19]. At large values of k (or KR_m) the critical flux can be readily obtained from equation (30)

$$\omega_{cr}=(-\sin\theta)\max_S\left\{\frac{k_{rL}k_{rV}}{(k_{rL}+\beta k_{rV})}\right\} \tag{52}$$

(see also ref. [19]), a value largely independent of process parameters. In the more general case, however, a more elaborate approach is required.

To proceed, the problem described by equations (8)–(27) was solved using a numerical scheme based on stiff ODE IMSL solvers, the integration starting from region I and consecutively marching through regions II and III. Standard runs were carried out at the conditions of Table 1. Subsequently, a systematic numerical study was undertaken. As anticipated, results consistent with refs. [18, 19] were obtained in the limit of large KR_m. For example, in the more interesting case of bottom heating [19], critical heat flux values ω_{cr} were found, such that for $\omega/(-\sin\theta)>\omega_{cr}$, a two-phase zone exists of a length that decreases as ω increases. This behavior was thoroughly analyzed previously [19]. Unexplored in past investigations, however, were the effects of k and the nature of the solution for $\omega<\omega_{cr}$. While at large k (or KR_m), ω_{cr} approaches the asymptote (52), it was also found that it slowly increases with decreasing k, and it rapidly diverges when a critical permeability value k_b is approached (Fig. 3). This singular behavior was verified for a host of parameter values, the standard case yielding the estimate $k_b=144$ md, well within the range of natural reservoir rocks.

This interesting feature has not been noted before. For given conditions, a critical value k_b can be demarcated such that steady-state solutions are possible for $k>k_b$, in which case a minimum heat flux is required (region A in Fig. 5). The magnitude of the latter is not constant as previously held, although it approaches at large k the asymptote (52). In the opposite case, $\omega<\omega_{cr}$ or $k<k_b$, saturation and temperature profiles are ill-behaved, in a manner to be specified below, and the existence of steady-state solutions must be questioned.

To analyze the critical heat flux at bottom heating, the nature of the solution for $\omega<\omega_{cr}$ must be examined. We consider a representative example with $k=10^{-12}$ m^2 and parameter values $S_{Lr}=S_{Vr}=0$. Here ($k>k_b$) the critical heat flux is $\omega_{cr}=0.45$, significantly larger than 0.306348 obtained from the estimate (52). Typical (τ, S) trajectories are shown in Figs. 4–6 for the values $\omega=0.1$, 0.4, and 0.5, respectively. Also plotted are the level curves when the numerator in equation (19) vanishes, $G(\tau, S)=0$, a

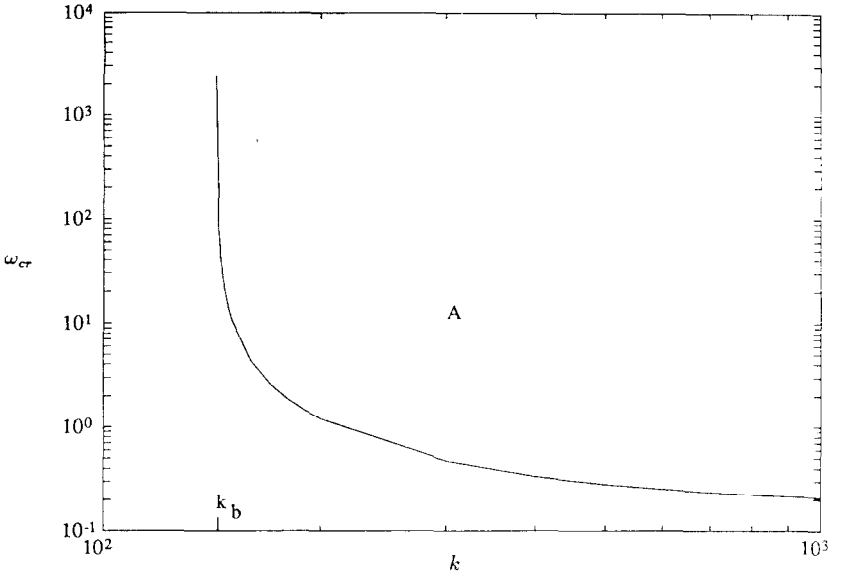

FIG. 3. Critical heat flux as a function of permeability for bottom heating.

condition necessary for the change of slope in the (τ, S) trajectory.

The first case (Fig. 4) is characteristic of one kind of ill-condition, namely that the domain $G > 0$ is disconnected and does not extend over the entire saturation interval. As a result, the solution trajectory changes slope at some point (A in Fig. 4), and further penetration into the two-phase region leads to progressively higher steam saturation and unphysically low temperatures. Previous investigators [17, 19] suggested that a two-phase zone of 'infinite' length would develop under such conditions. While it is true that the penetration depth for a given saturation is significantly higher and in fact it should increase even more as KR_m increases (both the trajectory and the $G = 0$ level curve become steeper in the latter case), unrealistically low temperatures and vapor pressures are eventually reached and the two-phase zone terminates at non-physical values. We argue against the existence of a steady state under such conditions.

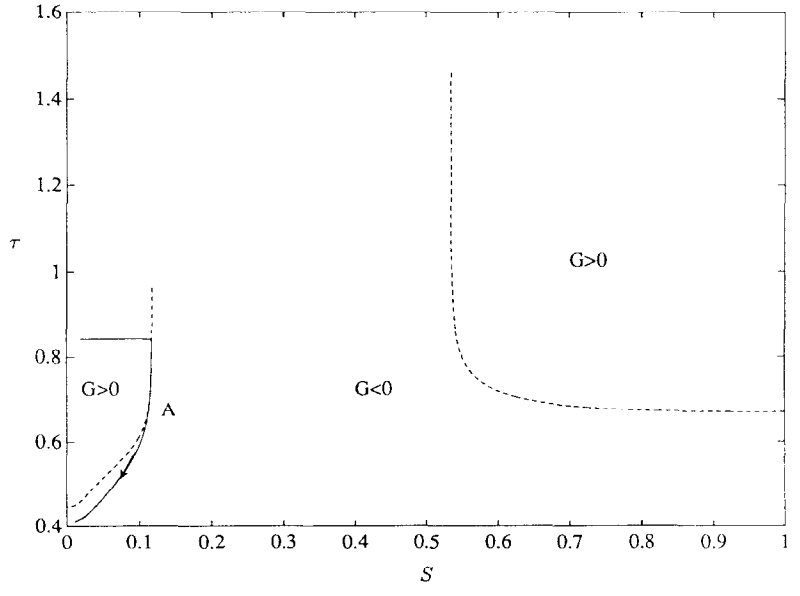

FIG. 4. Temperature vs saturation solution trajectories for bottom heating and $\omega = 0.1$: the dashed curves correspond to $G = 0$.

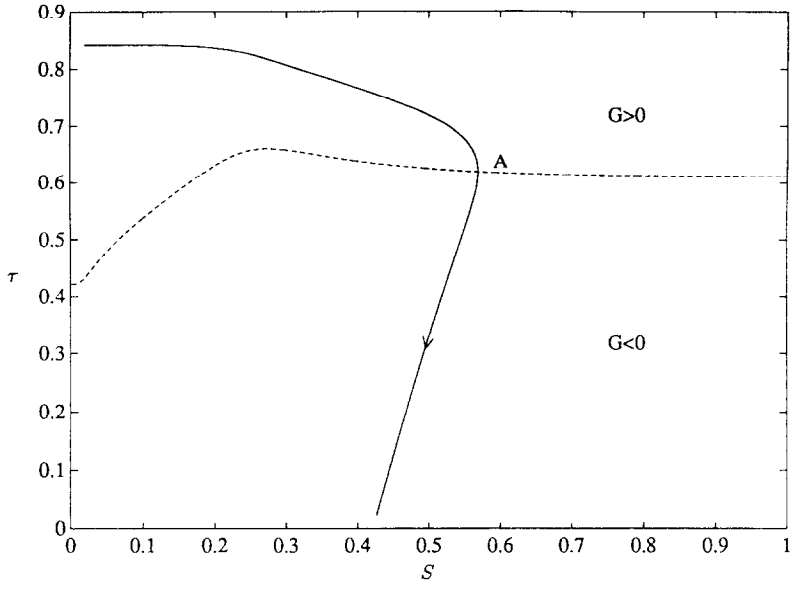

FIG. 5. Temperature vs saturation solution trajectories for bottom heating and $\omega = 0.4$: the dashed curve corresponds to $G = 0$.

The second case (Fig. 5) is characteristic of a different kind of ill-condition. Although the domain $G > 0$ spans the entire saturation interval $(0, 1)$, the value of ω is not high enough, thus the (τ, S) trajectory intersects the $G = 0$ curve before it reaches the end of the two-phase zone. This condition is entirely due to the finite value in KR_m, the no-conduction model predicting no pathological behavior for $\omega > 0.306348$, as pointed out above. At the point of intersection A, the saturation profile has a turning point and the ill-condition of the previous case is encountered. On the other hand, for sufficiently large values of ω, the two curves are at large enough distance, such that the solution trajectory terminates at the end of the two-phase zone before intersection, and a true heat pipe is established (Fig. 6). Smaller values in k lead to increasingly larger critical heat flux values and, at least within a certain range of k away from k_b, the above interpretation of the ω_{cr} vs k curve applies.

While the departure of ω_{cr} from the asymptote (52) was attributed primarily to conduction, near the threshold region ($k \sim k_b$) capillarity becomes predominant. The condition determining ω_{cr} still remains the same, namely that a turning point (where $G = 0$) in the saturation profile develops. It was numerically observed that the latter first occurs at the end of the two-phase zone, where $S \to 1 - S_{Vr}$ and $k_{rV} \to 0$. Substitution in $G = 0$ yields after manipulation of equation (22)

$$\frac{\omega_{cr}}{-\sin\theta} \simeq \frac{1}{KR_m}\left(\frac{\tau^2}{A}\right)_2 \gg 1 \tag{53}$$

where ω_{cr} was assumed large. Indeed, as k approaches k_b, ω_{cr} becomes infinitely large, which, in view of the finite value of KR_m, must be attributed to the vanishing of the vapor pressure A_2. An estimate of the vapor pressure at the large ω limit can be obtained from equations (18) and (19)

$$R_p \frac{KA}{\tau^2}\frac{d\tau}{dS} = \frac{dJ}{dS}\frac{k_{rL}}{(k_{rL}+\beta k_{rV})} \tag{54}$$

which can be further integrated to

$$R_p(A_2 - A_1) \simeq \int_{S_{Lr}}^{1-S_{Vr}} \frac{k_{rL}J'(S)\,dS}{(k_{rL}+\beta k_{rV})}. \tag{55}$$

We note that as expected, this is also the limit of equation (44) for the case of horizontal heating ($\sin\theta = 0$). We conclude that the critical threshold k_b can be determined by simply taking in expression (55) the limit $A_2 \ll 1$

$$k_b \simeq \left(\frac{\sigma}{P_0}\right)^2\left[\int_{S_{Lr}}^{1-S_{Vr}}\left(-\frac{dJ}{dS}\right)\frac{k_{rL}\,dS}{(k_{rL}+\beta k_{rV})}\right]^2. \tag{56}$$

Thus, while the behavior of the critical flux near the two threshold regions is significantly influenced by conduction (see expression (53)), the permeability threshold k_b is solely dictated by capillarity. The analytical expression (56) contains all features observed in our numerical investigations. Thermal conductivity was found to have no effect on k_b, although it significantly influences the shape and magnitude of the critical curve. A sensitivity, generally weak, with respect to the residual saturations (which lead to a decrease of the overall permeabilities in the model of

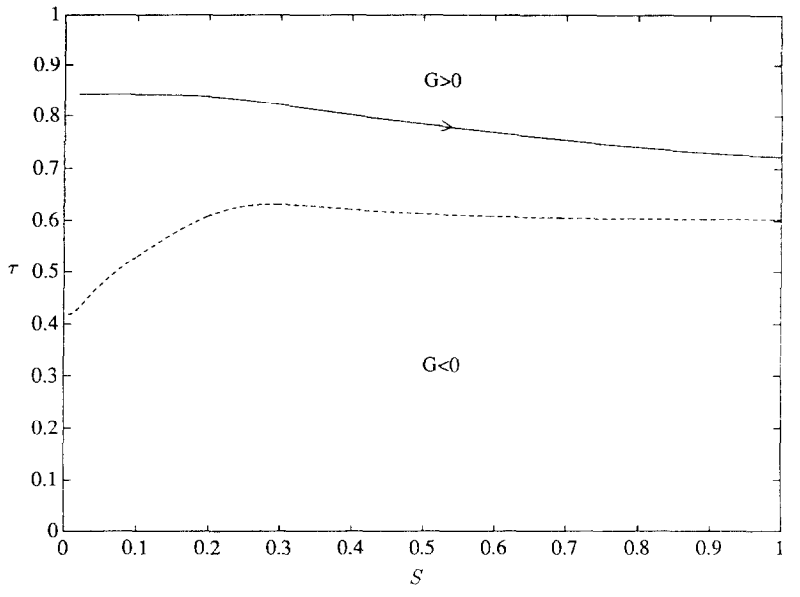

FIG. 6. Temperature vs saturation solution trajectories for bottom heating and $\omega = 0.5$: the dashed curve corresponds to $G = 0$.

Table 1). Most significant, however, are the effects of capillarity and the imposed pressure P_0, the threshold value varying in proportion to the square of σ/P_0. While substantial changes in σ mainly require changes in the fluid chemistry, large variations in P_0 can be readily accomplished. Therefore, a wide variation in k_b is possible. For the typical conditions of laboratory experiments with heat pipes, relatively high thresholds should be expected. By contrast, very small k_b values (of the order of 10^{-17} m^2) would be obtained for geothermal systems. The agreement between numerical and analytical results is excellent.

For completeness, and after additional algebra, an estimate of the critical curve near k_b may also be derived

$$\frac{\omega_{cr}}{-\sin\theta} \sim \frac{(\text{const})}{KR_m(k-k_b)(\ln|k-k_b|)^2}. \qquad (57)$$

The latter contains, through R_m, observed effects of the thermal conductivity, λ. As previously remarked, conductivity does not affect the threshold value, although it influences the shape of the critical curve.

Although the above pertains to bottom heating, essentially similar results were numerically obtained for the case of top heating, as well. As expected, no constraint in the process parameters was found for sufficiently large k. At smaller permeability values, however, a sensitivity similar to the case of bottom heating was detected and a similar (although not as sharp) threshold value, k_t, was identified. Now, steady states are possible for any heat flux value, if $k > k_t$, and for sufficiently low heat flux values, $\omega < \omega_{cr}$ if $k < k_t$ (region A in Fig. 7). When these conditions are not satisfied (region B in Fig. 7), a steady-state counterflow may not be sustained. Sensitivity studies revealed features similar to the case of bottom heating. Capillarity and imposed pressure P_0 were found to be the most important variables. In fact, the two thresholds k_t and k_b were found to practically coincide. Likewise, the onset of critical behavior coincides with unphysically low temperatures, first encountered at the end of the two-phase region. In the limit $1 \ll \omega < \omega_{cr}$, it can be easily shown that the previous analysis, notably results (56) and (57), apply. To provide a better pictorial, the composite of ω_{cr} near the threshold region was constructed (Fig. 8). For the case of top heating ($0 < \theta < \pi$), steady-state solutions are possible within the 'tunnel' at the front-left, the cross-section of which expands to an infinitely large value when $k > k_b$. Conversely, for bottom heating ($\pi < \theta < 2\pi$), steady states can be sustained only outside the 'tunnel' at the back-right, the cross-section of which also diverges when $k < k_b$.

We shall conclude this section by providing an alternative physical interpretation of the threshold condition (57). For this, we first consider the horizontal case, $\theta = 0$, which demarcates the boundary between top and bottom heating. For negligible Kelvin and other secondary effects, the two-phase flow region starts when the vapor becomes saturated, $P_V = P_0$. Counterflow in this region is possible only because of capillarity. In fact, the changes in vapor pressure and capillary pressure are interrelated

$$dP_V = \frac{k_{rL}}{k_{rL} + \beta k_{rV}} dP_c. \qquad (58)$$

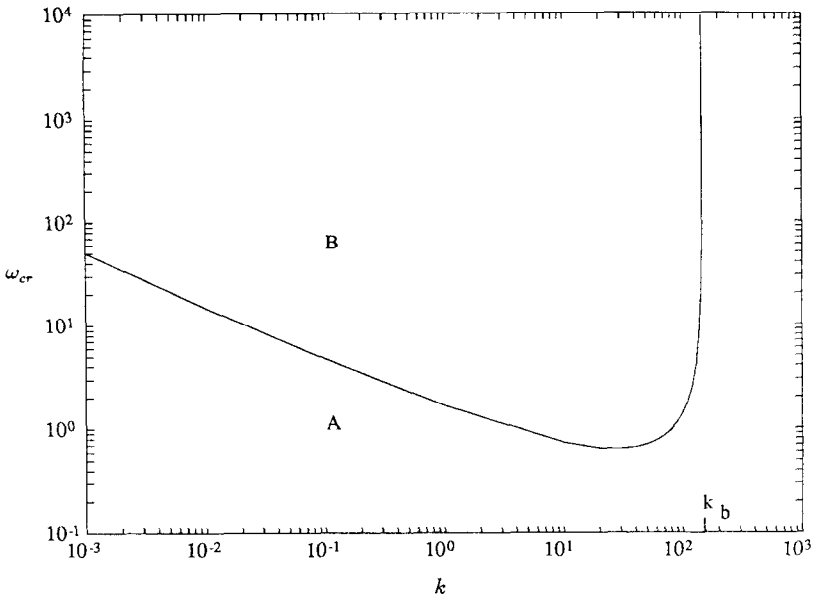

FIG. 7. Critical heat flux as a function of permeability for top heating.

As long as capillarity is small, the vapor pressure drop across the region

$$P_V = P_0 - \int_0^{P_c(S_{1r})} \frac{k_{rL}}{k_{rL} + \beta k_{rV}} \, dP_c \qquad (59)$$

is not large and $P_V > 0$. Problems arise when the permeability is low, such that capillarity is large enough for the right-hand side above to become negative. It is straightforward to show that the onset of this condition is at the above threshold, k_b. Below this value, capillarity is large, thus negative values for P_V result. Clearly, k_b (or k_1) also denotes the lowest permeability value below which steady-state, horizontal counterflow cannot be sustained.

When the medium is inclined, gravity opposes or supplements capillarity, depending on whether the vapor overlies or underlies the liquid. For instance, the expression equivalent to equation (59) is

$$P_V = P_0 - \int_0^{P_c(S_{1r})} \frac{k_{rL}}{k_{rL} + \beta k_{rV}} \, dP_c + \rho_L g \sin\theta \int_{x_2}^{x_1} I \, dx \qquad (60)$$

where

$$I = \frac{k_{rL} + \beta R_v k_{rV}}{k_{rL} + \beta k_{rV}}. \qquad (61)$$

When heating is from the top, capillary pressure is counterbalanced by adverse gravity effects, and a two-phase region may exist even for $k < k_1$, provided that the heat flux is small enough. One may recall that the extent of the two-phase zone increases as the heat flux decreases. Opposite considerations apply for the case of bottom heating. At least near k_b, gravity would supplement capillarity in increasing pressure drops, with a contribution roughly proportional to the extent of the two-phase zone. At low $\omega < \omega_{cr}$, the latter is of large enough extent, thus a steady state cannot be sustained.

One concludes that consideration of conduction and lower permeability values in the heat pipe problem leads to unexpected, and non-trivial corrections, particularly for the case of bottom heating. The relevance of the threshold k_b to heat pipe problems which place emphasis on capillarity cannot be discounted. A measure of the latter is the parameter R_p. For values of R_p of order 1 or less, the obtained k_b value is of the same order with the medium permeability (compare equation (56)), and the problems analyzed above are likely to be encountered in such heat pipes. This is in contrast to geothermal problems, where capillarity is usually negligible (large values of R_p).

GEOTHERMAL PROBLEM

The second part of this paper addresses the geothermal version of the vapor–liquid counterflow, specifically the problem considered by Martin *et al.* [15] and Schubert and Straus [16]. Here $0 < \theta < \pi$, but the heating is from the bottom, thus, in our notation, the imposed temperature gradient and heat flux are negative (in the direction from the liquid to the vapor). We shall take reference values corresponding to the liquid two-phase zone interface, where for simplicity $S_{Vr} = 0$ will be assumed. Integration proceeds in the positive ξ-direction, from the liquid towards the vapor. The condition derived in ref. [16] is also recalled that the underlying liquid be

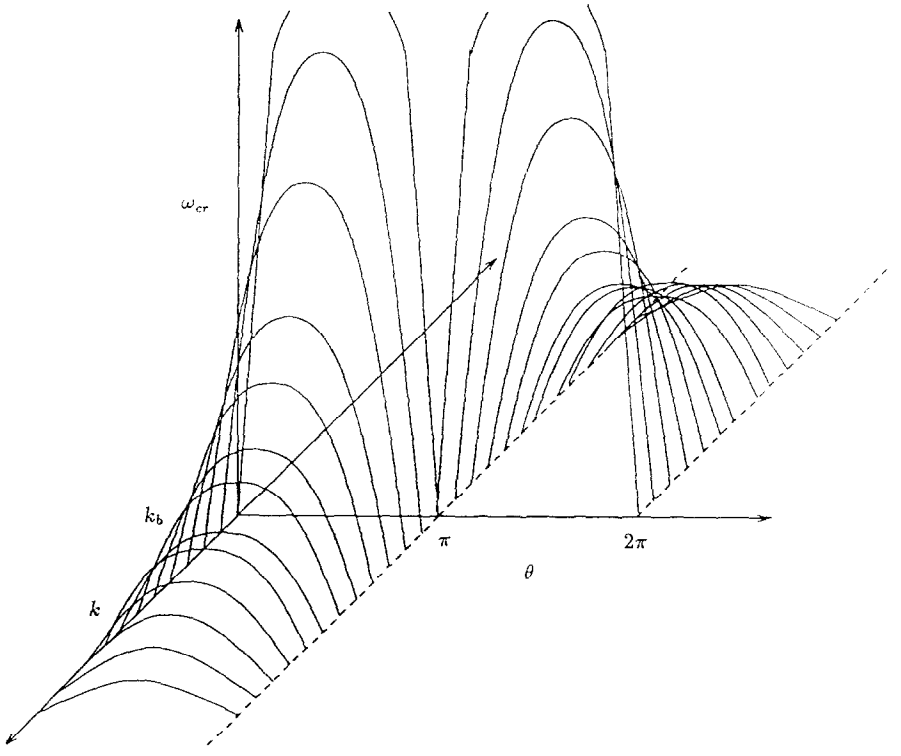

FIG. 8. Composite schematic of critical heat flux curve for both top and bottom heating.

subcooled, hence the temperature gradient or the heat flux may not exceed an upper limit. In our notation one obtains the equivalent condition

$$-\omega < \frac{R_l}{KR_m} \sim \frac{1}{KR_m}. \tag{62}$$

As previously discussed, the geothermal version of the counterflow formulation (18)–(22) is obtained at the following (no-capillary) limit in the absence of Kelvin effects

$$KR_p \gg 1. \tag{63}$$

With reference conditions corresponding to the top of the liquid zone, the above condition reads as follows:

$$\frac{L_v P_{ll} M_w}{RT_0} \gg \frac{\sigma}{\sqrt{k}}. \tag{64}$$

Consistent with refs. [15, 16], conditions (63) or (64) imply that capillarity is of secondary importance and sharply differentiate geothermal and heat pipe problems. To proceed we recast equations (18)–(22) in the form

$$\frac{d\tau}{dS} = -\varepsilon \frac{k_{rL}[KR_m(-\omega) + KR_m R_v k_{rV}]\dfrac{dJ}{dS}}{G(\tau, S)} \tag{65}$$

$$\frac{dS}{d\xi} = -\frac{G(\tau, S)}{k_{rL}\left[1 + KR_m \dfrac{A}{\tau^2} k_{rV}\right]\dfrac{dJ}{dS}} \tag{66}$$

where we denoted $\varepsilon = 1/KR_p$ and the expression for G, equation (22), has been rewritten as

$$G(\tau, S) = k_{rl}\left[R_l + KR_m\omega\frac{A}{\tau^2} + KR_m\frac{A}{\tau^2}k_{rV}\right] + \beta k_{rV}\left[R_v + KR_m\omega\frac{A}{\tau^2}\right]. \tag{67}$$

As in the heat pipe problem it is convenient to characterize the solution of the problem using solution trajectories (Figs. 9 and 10). Of particular importance in this respect is the critical curve where $G(\tau, S) = 0$ (Fig. 9). In general, G and $KR_m\omega$ are of $O(1)$ or less (compare with expression (62)). Thus, in the limit $\varepsilon \ll 1$, solution trajectories (τ, S) have constant temperature $(d\tau/dS \cong 0)$, in regions where G is not small, and closely follow the $G = 0$ curve, otherwise (compare with equation (65), Fig. 9). In the region of constant temperature, the saturation changes rapidly over an interval of $O(1)$ in length (Fig. 10) (which, as recalled, expresses a balance between gravity and capillarity in the present notation). It is in this region (taken as a sharp interface in previous works [15, 16]), where capillarity influences the saturation profile.

Significant temperature changes start occurring when the solution trajectory approaches the curve $G(\tau, S) = 0$. For the conditions of Fig. 9, the latter interval (AB in Fig. 9) is the vapor-dominated regime analyzed by Schubert and Straus [16] for a simpler

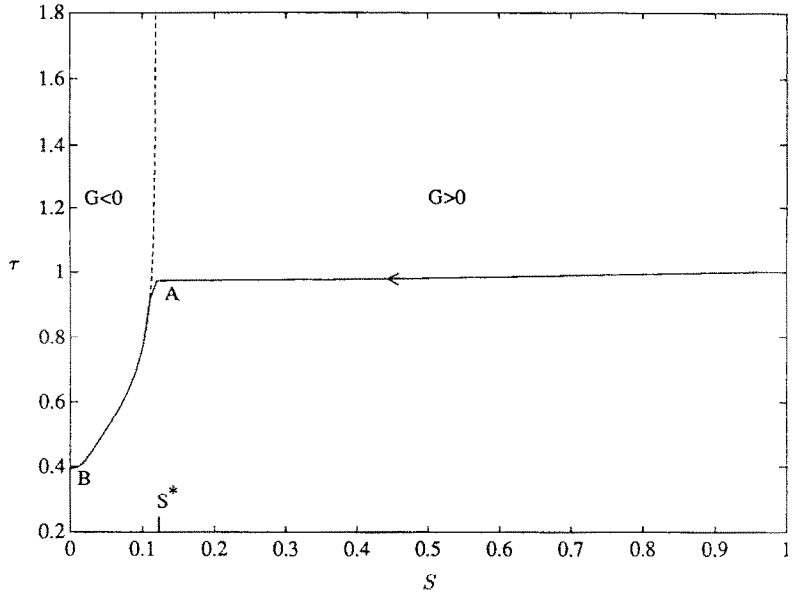

FIG. 9. Temperature vs saturation solution trajectories for the geothermal problem and $\varepsilon = 0.0265275$: the dashed curve corresponds to $G = 0$.

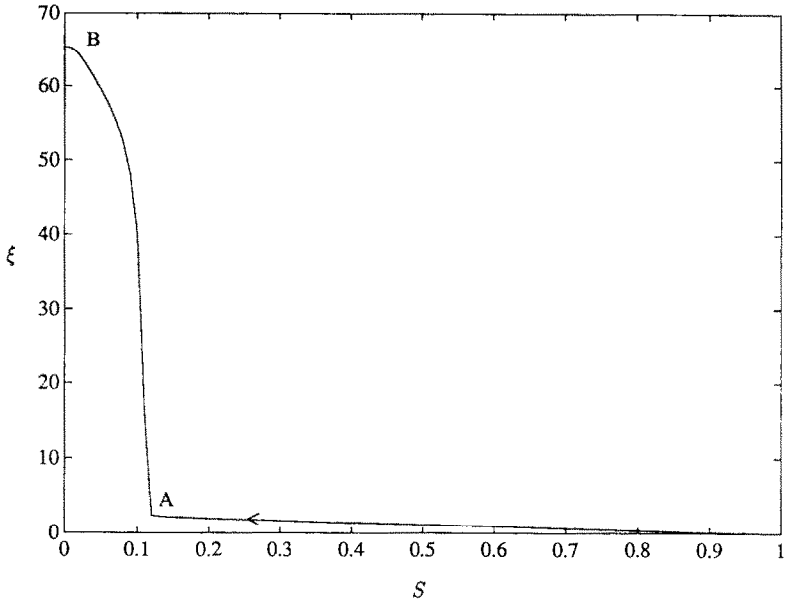

FIG. 10. Saturation vs distance for the geothermal problem and $\varepsilon = 0.0265275$.

model involving straight-line relative permeabilities. As is apparent from equation (66), in this domain, the saturation gradient is very small ($G \ll 1$) thus, the spatial extent of the region is quite large (Fig. 10). In the limit $\varepsilon \ll 1$, the region commences at saturation S^* (approximately at point A) satisfying $G(1, S^*) = 0$, a condition previously derived although in a different notation [16]. At larger values of ε, however, capillarity can become important and must be also considered (Fig. 11). Here, although ultimately attracted to the curve $G(\tau, S) = 0$, the solution trajectory shows substantial temperature variation before the vapor-dominated region is entered.

With an approximation that rapidly improves as ε diminishes, the previous analysis [16] describes the behavior of steam–water counterflow in the geothermal context with excellent accuracy. Considerations similar to ref. [16] were also advanced by

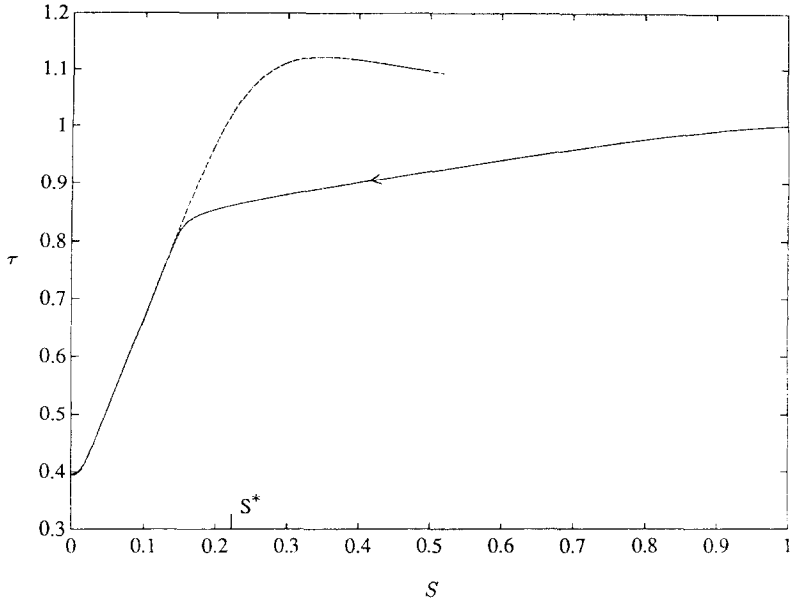

FIG. 11. Temperature vs saturation solution trajectories for the geothermal problem and $\varepsilon = 0.0838876$: the dashed curve corresponds to $G = 0$.

Martin *et al.* in an earlier publication [15]. While also identifying the vapor-dominated regime, they have additionally proposed the existence of liquid-dominated regions. The present formulation readily yields such solutions as well. For this, it is required that the equation $G(1, S^*) = 0$ admits two solutions, a condition that can be met at higher values in ω.

At such conditions, the (τ, S) diagram is divided into three regions (two far regions with $G < 0$ and a middle one with $G > 0$) by the two branches of the curve $G = 0$ (Fig. 12). The theory proposed earlier [15] can then be rephrased as follows in the present context: vapor- or liquid-dominated regimes commence at point A or B, respectively, where $G(1, S^*) = 0$, and they subsequently follow the respective branches of $G(\tau, S) = 0$ (paths AV, BL, respectively). Such behavior appears consistent with equations (65) and (66) in the limit $\varepsilon \ll 1$, but it is doubtful that it actually materializes at steady state, for the following reasons.

By definition, a solution trajectory must originate from the top of the liquid zone (point C, where $\tau = 1$, $S = 1$ and $G < 0$), other starting conditions being impossible in a steady-state counterflow system. This trajectory has a slightly negative slope and approaches the $G = 0$ branch to which it rapidly becomes parallel (dashed-line path CD in Fig. 12). Somewhat analogous to the heat pipe problem, the solution trajectory crosses over to the middle region ($G > 0$), acquires positive slope and parallels the branch $G = 0$ from the other side (note that the two curves practically coincide in Fig. 12). The immediate implication is that the trajectory suggested earlier (path BL) may not be acceptable.

While being different than previously proposed (path BL), the other alternative solution (path CD) is not acceptable either. An inspection of equation (66) readily reveals that ξ must decrease along path CD, contradicting the requirement that, by convention, ξ increases in the direction from the 'liquid' to the 'vapor'. The other alternative, namely the trajectory extending from point C in the direction opposite to B, is also rejected as it leads to saturation values larger than one. It becomes evident that under such high heat flux conditions, a liquid-dominated regime of this type is not realistic, while the associated vapor-dominated regime is also never reached, certainly not when the starting point is the top of the liquid zone, as assumed throughout. One is led to conjecture that for such cases, which require that the heat flux exceed a certain value, steady-state solutions are not possible. The limiting heat flux is easily determined to be the upper bound (62), which, as recalled, sets the necessary condition for the underlying liquid to be subcooled. This limitation, inherent to any such problem, serves to reinforce the above conclusion.

A final remark is also appropriate regarding the analysis presented by Bau and Torrance [17]. These authors examined a configuration with $\theta = 3\pi/2$ and bottom heating (steam at the bottom, temperature gradient in the direction from the vapor to the liquid zone), a problem analyzed in the heat pipe section. In addition to conduction, however, they also neglected capillarity. Because of the latter, some similarities with the geothermal problem may exist. In our formulation, their analysis corresponds to the conditions $KR_p \gg 1$, $KR_{in} \gg 1$. By simple rearrangement, equations (18)–(22) read for this problem

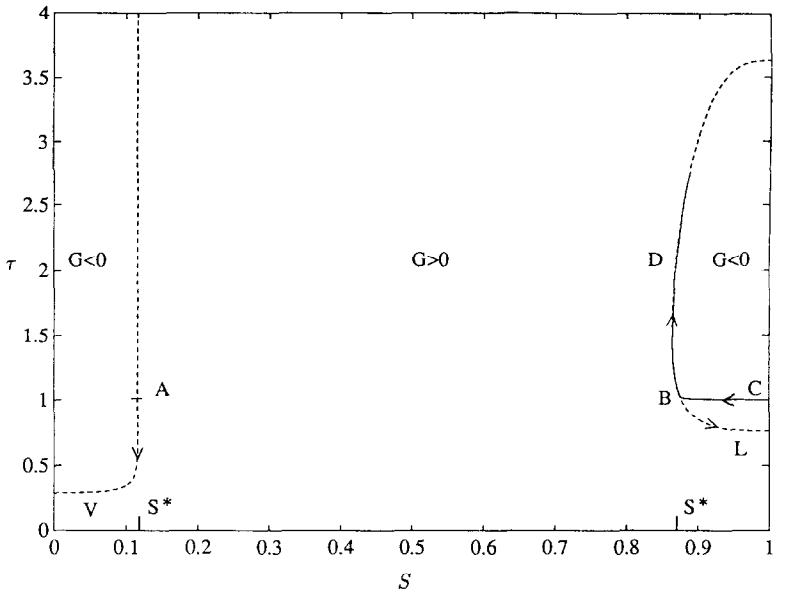

FIG. 12. Temperature vs saturation solution trajectories for the geothermal problem, with heat flux exceeding the limit (62): the dashed curves correspond to $G = 0$.

$$\frac{d\tau}{dS} = \varepsilon \frac{k_{rL}(\omega + k_{rV}R_v)\dfrac{dJ}{dS}}{G(\tau, S)\dfrac{A}{\tau^2}} \tag{68}$$

$$\frac{dS}{d\xi} = \frac{G(\tau, S)}{k_{rL}k_{rV}}\frac{dS}{dJ} \tag{69}$$

where $\varepsilon = 1/KR_p$, and the function $G(\tau, S)$ here simplifies to

$$G(\tau, S) = (k_{rL} + \beta k_{rV})\omega - k_{rL}k_{rV}. \tag{70}$$

It readily follows that, despite the small capillary effects, the problem is of the same nature as that of the heat pipe thoroughly analyzed before. Thus, identical conclusions must be reached regarding solution trajectories and the critical heat flux value, ω_{cr}, which is the necessary lower limit for the existence of a steady-state, steam–water counterflow. Under the implied assumption of negligible conduction, $KR_m \gg 1$, this critical value coincides with the asymptote (52).

CONCLUSIONS

In this paper we have attempted to unify the description of a diverse set of problems arising in heat pipe and geothermal contexts that contain the common process of steady-state, vapor–liquid counterflow. The formalism introduced encompasses several previous studies, which arise as special cases at various limits. In particular, a quantitative assessment of the importance of gravity, capillarity, phase equilibria, heat conduction and Kelvin effects becomes possible. A similar approach was also recently implemented for the case of vapor–liquid concurrent flow [27].

In the context of the heat pipe problem, it was shown that Kelvin effects are of significance only over a narrow boundary layer at the vapor–two-phase boundary, and are otherwise negligible in the counterflow region. Heat conduction was found to influence saturation and temperature profiles near the other end of the two-phase region. It was conjectured that for the case of bottom heating, steady-state counterflow is not possible when the heat flux is below a critical value. Contrary to previous results, the latter is constant only in the limit of large permeability. A permeability threshold value k_b was identified, such that no steady-state counterflow can exist for media of lower permeability. The threshold reflects capillary effects and is mainly a function of the imposed pressure.

The geothermal problem was similarly analyzed. The results of Schubert and Straus [16], where capillarity is neglected, were recovered as a limiting case of the present formulation. The same limit is also applicable for the cases discussed by Martin *et al.* [15]. However, the liquid-dominated regime of the latter was found to lead to non-physical predictions, and it was suggested that such a steady state may not be reached, at least not for homogeneous reservoirs. It is hoped that the present analysis clarifies several of the issues involved in steady-state, vapor–liquid counterflow, and that it may be useful for further studies in this area.

Acknowledgement—This work was partly supported by DOE Contract DE-FG19-87BC14126, the contribution of which is gratefully acknowledged.

REFERENCES

1. D. E. White, L. J. Muffler and A. H. Trusdell, Vapor-dominated hydrothermal systems compared with hot-water systems, *Econ. Geol.* **66**(1), 75–97 (1971).
2. C. H. Sondergeld and L. Turcotte, An experimental study of two phase convection in a porous medium with applications to geological problems, *J. Geophys. Res.* **82**, 2045–2053 (1977).
3. G. Schubert and J. M. Straus, Two-phase convection in a porous medium, *J. Geophys. Res.* **82**, 3411–3421 (1977).
4. N. E. Bixler and C. R. Carrigan, Enhanced heat transfer in partially-saturated hydrothermal systems, *Geophys. Res. Lett.* **13**, 42–45 (1986).
5. M. Prats, *Thermal Recovery*, SPE Monograph, Vol. 7. Dallas, Texas (1982).
6. C. Doughty and K. Pruess, A semianalytical solution for heat-pipe effects near high-level nuclear waste packages buried in partially saturated geological media, *Int. J. Heat Mass Transfer* **31**, 79–90 (1988).
7. J. M. Buchlin, Transport processes associated with nuclear reactor safety, *Proc. NATO/ASI on Transport in Porous Media*, Pullman, Washington, 9–18 July (Edited by Y. Corapcioglu and J. Bear) (1989).
8. E. E. Gomma and W. H. Somerton, The behavior of multifluid-saturated formations, Part II: effect of vapor saturation-heat pipe concept and apparent, thermal conductivity, SPE Paper 4896-B, *Proc. Soc. Petroleum Engrs. California Regional Meeting*, San Francisco, April (1974).
9. Y. Ogniewicz and C. L. Tien, Porous heat pipe. In *Heat Transfer, Thermal Control and Heat Pipes* (Edited by W. B. Olstad), 70, Progress in Astronautics (Series Editor M. Summerfield), pp. 329–345. AIAA, New York. Presented as paper 79-1093, AIAA 14th Thermophysics Conf., Orlando, Florida, June (1979).
10. V. Dhir and I. Catton, Dryout heat fluxes of inductively heated particulate beds, *J. Heat Transfer* **99**, 250–256 (1977).
11. E. R. G. Eckert, R. J. Goldstein, A. I. Behbahani and R. Hain, Boiling in an unconstricted granular medium, *Int. J. Heat Mass Transfer* **28**, 1187–1196 (1985).
12. K. Cornwell, B. G. Nair and T. D. Patten, Observation of boiling in porous media, *Int. J. Heat Mass Transfer* **19**, 236–238 (1976).
13. T. M. Shaw, Drying as an immiscible displacement process with fluid counterflow, *Phys. Rev. Lett.* **59**, 1671 (1987).
14. F. G. Miller, Steady flow of two-phase single-component fluids through porous media, *Petroleum Trans., AIME* **192**, 205 (1951).
15. J. C. Martin, R. E. Wegner and F. J. Kelsey, One-dimensional convective and conductive heat flow, *Proc. Second Workshop Geothermal Reservoir Engng*, 1–3 December (1976).
16. G. Schubert and J. M. Straus, Steam–water counterflow in porous media, *J. Geophys. Res.* **84**, 1621 (1979).
17. H. H. Bau and K. E. Torrance, Boiling in low-permeability porous materials, *Int. J. Heat Mass Transfer* **25**, 45–54 (1982).
18. K. S. Udell, Heat transfer in porous media heated from above with evaporation, condensation and capillary effects, *J. Heat Transfer* **105**, 485–492 (1983).
19. K. S. Udell, Heat transfer in porous media considering phase change and capillarity—the heat pipe effect, *Int. J. Heat Mass Transfer* **28**, 485–495 (1985).
20. M. Parlar and Y. C. Yortsos, Percolation theory of steam–water relative permeability, paper SPE 16969 presented at the 62nd Annual Meeting of SPE, Dallas, Texas, 27–30 September (1987).
21. S. Whitaker, Heat and mass transfer in granular porous media. In *Advances in Drying* (Edited by A. S. Majumdar), Chap. 2, Vol. 1. Hemisphere, Washington, DC (1980).
22. Y. C. Yortsos and M. Parlar, Phase change in porous media: application to solution gas drive, paper SPE 19697 presented at the 64th Annual Technical Conf. and Exhibition of SPE, San Antonio, Texas, 8–11 October (1989).
23. F. Kalaydjian, A macroscopic description of multi phase flow in porous media involving spacetime evolution of fluid/fluid interface, *Transp. Porous Media* **2**, 537–552 (1987).
24. J. C. Melrose, Use of water vapor desorption data in the determination of capillary pressures, *SPE Reservoir Engng* 913–919 (1988).
25. P. D. de Gennes, *Physics of Disordered Materials* (Edited by D. Adler, H. Fritz and S. R. Ovshinsky). Plenum Press, New York (1985).
26. C. M. Bender and S. A. Orszag, *Advanced Mathematical Methods for Scientists and Engineers*. McGraw-Hill, New York (1978).
27. M. Parlar, M. Zeybek and Y. C. Yortsos, Steady-state, vapor–liquid concurrent flow: relative permeabilities and end-effects, paper SPE 20054 presented at the SPE California Regional Meeting, Ventura, California, 4–6 April (1990).

APPENDIX

The dimensionless constants c, e, f are obtained by a straightforward analysis. We obtain

$$c = \frac{\beta R_p A_1 k_{rV}(S_{Lr})}{1 + k_{rV}(S_{Lr}) K R_m \dfrac{A_1}{\tau_1^2}} \tag{I}$$

$$e = \frac{R_s + K R_p R_h \dfrac{A_1}{\tau_1^2}}{R_p A_1 J'(S_{Lr})} \tag{II}$$

$$f = -\frac{nL}{\beta} J'(S_{Lr}) e^2 \tag{III}$$

where A_1 and τ_1 pertain to conditions at ξ_1. For typical parameter values [18] and $k = 10^{-12}$ m^2, we obtain the estimates

$$c = 2.469 \times 10^{-4}, \quad e = 80.5169, \quad f = 3.0981 \times 10^{6}.$$

UNE ETUDE DU CONTRECOURANT PERMANENT VAPEUR–EAU LIQUIDE DANS LES MILIEUX POREUX

Résumé—Le contrecourant vapeur–liquide dans les milieux poreux apparait dans les mécanismes de caloducs, récupération d'huile brute et les systèmes géothermiques. Alors que les études précédentes analysaient ces mécanismes séparément, on présente ici une description unique. L'analyse inclut la capillarité, la conduction de chaleur et les effets de Kelvin. L'importance de chaque terme est examinée dans les différentes applications. On trouve que le flux de chaleur critique dans un caloduc n'est pas constant mais qu'il augmente quand la perméabilité diminue. On identifie un seuil de perméabilité au dessous duquel des états permanents ne peuvent exister. Des conclusions sont tirées concernant les systèmes géothermiques dominés par le liquide.

UNTERSUCHUNG DER STATIONÄREN GEGENSTRÖMUNG VON DAMPFFÖRMIGEM UND FLÜSSIGEM WASSER IN EINEM PORÖSEN MEDIUM

Zusammenfassung—Die Gegenströmung von Dampf und Flüssigkeit in porösen Medien kommt beispielsweise in Wärmerohren, bei der Ölrückgewinnung und in geothermischen Systemen vor. Im Gegensatz zu früheren Untersuchungen, in denen diese Prozesse getrennt analysiert worden sind, wird in der vorliegenden Arbeit eine einheitliche Beschreibung vorgestellt. Dabei werden die Kapillarwirkung, die Wärmeleitung sowie Kelvin-Effekte berücksichtigt. Die Bedeutsamkeit der einzelnen Terme bei den einzelnen Anwendungen wird untersucht. Es ergibt sich, daß die kritische Wärmestromdichte in einem Wärmerohr nicht konstant ist, sondern mit abnehmender Permeabilität zunimmt. Es wird auch ein Schwellenwert für die Permeabilität ermittelt, unterhalb dem stationäre Zustände nicht möglich sind. Entsprechende Schlußfolgerungen ergeben sich für flüssigkeitsgesteuerte geothermische Systeme.

ИССЛЕДОВАНИЕ СТАЦИОНАРНОГО ПРОТИВОТОКА ПАРА И ВОДЫ В ПОРИСТЫХ СРЕДАХ

Аннотация—Противоток пара и жидкости в пористых средах возникает в тепловых трубах при регенерации масла, а также в геотермальных системах. В отличие от предыдущих исследований, анализирующих эти процессы по отдельности, в данной статье представлено обобщенное описание. Анализ учитывает капиллярность, теплопроводноость и эффект Кельвина. Рассматривается значение каждого из этих эффектов в различных приложениях. Сделан важный вывод о том, что критический тепловой поток в тепловой трубе не является постоянным, а увеличивается с уменьшением проницаемости. Определена пороговая проницаемость, ниже которой стационарные состояния могут не существовать. Сделаны также заключения относительно геотермальных систем, в которых доминирует жидкость.